NJC

ROYAL SOCIETY OF CHEMISTRY

PAPER

View Article Online
View Journal | View Issue

Cite this: *New J. Chem.*, 2024, **48**, 16261

Molecularly rigid porous polyamine host enhances barium titanate catalysed H_2O_2 generation†

Akalya Karunakaran,[ab] Chris R. Bowen,[b] Steve Dunn,[c] Thuy-Phuong T. Pham,[de] Andrea Folli,[f] Philip J. Fletcher,[g] Mariolino Carta,[h] Neil B. McKeown[i] and Frank Marken*[a]

Received 3rd August 2024,
Accepted 2nd September 2024

DOI: 10.1039/d4nj03460k

rsc.li/njc

Barium titanate (BTO) is well-known (as a photo- or sono/piezo-catalyst) to produce hydrogen peroxide *via* 2-electron reduction of oxygen in the presence of a sacrificial quencher, such as isopropanol. While barium titanate nanoparticles with a tetragonal crystal structure (piezoelectric) are particularly reactive, the recovery and reuse of these nano-catalysts from reactions can be difficult. Here, barium titanate nanoparticles of typically 200 nm to 600 nm diameter are embedded into a host film of a polymer of intrinsic microporosity (PIM-EA-TB). Due to molecular rigidity of the polymer, there is no capping effect, and the surface catalytic reaction occurs effectively with a catalyst embedded in the polymer. In this exploratory work, the catalytic formation of H_2O_2 in the presence of isopropanol is investigated *via* kinetic studies and by electron paramagnetic resonance (EPR). Perhaps surprisingly, at a neutral pH the rate of the catalytic reaction is substantially increased when barium titanate is embedded into the polymer host and when the polymer is protonated. This is attributed here to a "kinetic cage effect" which exploits the tertiary amine in the polymer backbone with anodic and cathodic processes coupled into a pH neutral reaction.

1. Introduction

Barium titanate (BTO) is a phase-changing ferroelectric material.[1] Barium titanate has been employed as a catalyst in a range of potential applications; this has included piezo-photocatalysis,[2] water pollution treatment,[3,4] hydrogen production and anti-bacterial coatings,[5] in hydrogen peroxide formation and therapeutic applications,[6] and for bio-piezoelectric platforms.[7] In most cases, the catalytic process is suggested to be associated with piezoelectric effects,[8] namely it is linked to mechanically induced/enhanced electric fields at crystal surfaces that lower the activation barrier. The activation of barium titanate has been achieved by light,[9] by ultrasound,[10] or even by mechanical stirring.[11] Barium titanate is synthesised in the form of powders, or nanopowders, and is often simply added to the reaction. Here, the use and recovery of the barium titanate catalyst is attempted by embedding the catalyst nanopowder into a molecularly rigid microporous host polymer (PIM-EA-TB). In this regard, nanocomposites based on barium titanate in polymer hosts are of considerable interest.[12] Perhaps surprisingly, an enhanced catalytic reactivity is observed.

Polymers of intrinsic microporosity[13,14] (PIMs) have emerged over the past decade with intriguing properties due to a molecularly rigid structure enhancing processability (the poor intermolecular contact increases solubility) and inducing intrinsic microporosity with typically 1–2 nm diameter pores.[15] A prototypical PIM is PIM-EA-TB[16] ("EA" for ethanoanthracene and "TB" for Tröger base, see molecular structure in Fig. 1) with a typical BET surface area of 939 $m^2\ g^{-1}$ and a pore volume of approx. 0.9 $m^3\ g^{-1}$, depending on the degree of protonation.[17] The tertiary amine has been observed to be protonated at approx. pH 4. The molecularly rigid backbone of the polymer avoids nanoparticle surface capping[18] and ensures full accessibility and reactivity of the embedded nanocatalysts.[19] In fact, cages can form at the interface where the polymer can affect the catalytic reaction. Examples for applications of PIMs in catalysis include embedded photocatalysts for hydrogen generation,[20]

[a] *Department of Chemistry, University of Bath, BA2 7AY, Bath, UK. E-mail: f.marken@bath.ac.uk*
[b] *Department of Mechanical Engineering, University of Bath, BA2 7AY, Bath, UK*
[c] *London South Bank University, 103 Borough Road, London, SE1 0AA, UK*
[d] *Institute of Chemical Technology, Vietnam Academy of Science and Technology, 1A TL29 Street, Thanh Loc Ward, District 12, HCM City, Vietnam*
[e] *Graduate University of Science and Technology, Vietnam Academy of Science and Technology, 18 Hoang Quoc Viet Street, Cau Giay District, Hanoi, Vietnam*
[f] *School of Chemistry, Cardiff University, Cardiff, CF10 3AT, UK*
[g] *University of Bath, Imaging Facility, BA2 7AY, Bath, UK*
[h] *Department of Chemistry, Swansea University, College of Science, Grove Building, Singleton Park, Swansea SA2 8PP, UK*
[i] *EaStCHEM, School of Chemistry, University of Edinburgh, Joseph Black Building, David Brewster Road, Edinburgh, Scotland EH9 3JF, UK*

† Electronic supplementary information (ESI) available. See DOI: https://doi.org/10.1039/d4nj03460k

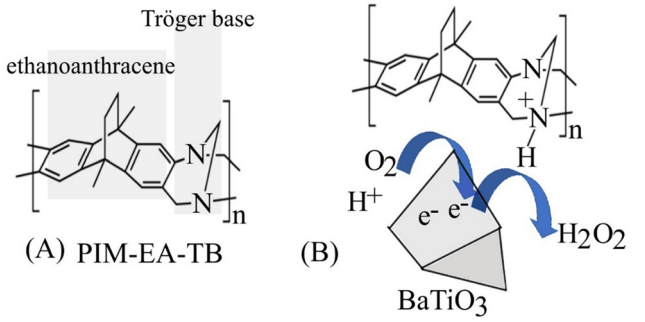

Fig. 1 (A) Molecular structure of PIM-EA-TB. (B) Illustration of $BaTiO_3$ catalyst reacting to produce hydrogen peroxide when embedded into PIM-EA-TB.

catalysis for hydrogen peroxide production,[21] and molecular catalysis for alcohol oxidation.[22] Usually, the PIM acts as an inert host in a similar way to zeolites or other inert host materials. However, in a recent report an example was presented whereby the use of PIM-EA-TB enhanced the catalytic conversion of formate oxidase activity.[23] It was suggested that in a two-step process the reduction of oxygen to hydrogen peroxide was enhanced by protonation of the tertiary amine within the PIM-EA-TB cages. A similar catalytic system is investigated here based on barium titanate.

The reduction of barium titanate leads to blue Ti(III) radical colour centres as observed by EPR spectroscopy[24] and by optical spectroscopy. In addition, barium titanate exists in distinct phases[25] due to temperature dependent symmetry-breaking of the high-temperature cubic perovskite phase and low-temperature tetragonal phase. The resulting interfacial strain and electric fields have been utilised in catalysis. In addition to pure barium titanate, cerium-doped barium titanate[26] and silver nanoparticle modified barium titanate materials[27] have been employed in enhanced piezo- and photocatalysis. Here, we demonstrate that barium titanate reactivity is enhanced by embedding into a porous polymer matrix.

There have been previous reports of barium titanate immobilisation into siloxane foams[28,29] and into PVDF[30] for water treatment applications. Here, barium titanate nanoparticles are investigated bare and when embedded into PIM-EA-TB. For the case of hydrogen peroxide production, it is demonstrated that the catalytic surface chemistry is retained and the polymer-embedded nanopowder is easily recovered and reused. A catalysis enhancing effect of the PIM-EA-TB cavity on hydrogen peroxide production is observed in acidic or neutral solution and assigned to enhanced dioxygen reduction.

2. Experimental

2.1. Chemical reagents

PIM-EA-TB $(C_{21}H_{20}N_2)_n$ with 1.08 g cm^{-3} was synthesised following a literature procedure.[31] Chloroform ($CHCl_3$, 1.49 g cm^{-3}, 119.38 g mol^{-1}, Sigma-Aldrich, >99% purity), isopropanol (C_3H_8O, 0.78 g cm^{-3}, 60.1 g mol^{-1}, Sigma-Aldrich, >99% purity), dimethyl sulfoxide ($(CH_3)_2SO_4$, 1.1 g cm^{-3}, 78.13 g mol^{-1}, Sigma-Aldrich, >99% purity), *para*-nitrophenyl boronic acid ($C_6H_6BNO_4$, 1.4 g cm^{-3}, 166.93 g mol^{-1}, Sigma-Aldrich, >99% purity), sodium bicarbonate ($NaHCO_3$, 2.2 g cm^{-3}, 84.007 g mol^{-1}, Sigma-Aldrich, >99% purity) were obtained commercially and used without further purification.

2.2. Barium titanate synthesis and characterisation

Barium titanate (BTO, $BaTiO_3$) was synthesised following a literature procedure[32] with an annealing step at 1000 °C; this annealing temperature led to maximum H_2O_2 production when compared to lower or higher annealing temperatures. Scanning electron microscopy images were recorded using a Jeol JSM-7900F field emission scanning electron microscope. The SEM images Fig. 2(a) and (b) data (Fig. 2) show particles of 0.37 ± 0.10 μm diameter. Transmission electron microscope images were recorded using a Jeol JEM-2100PLUS TEM. The fringe pattern in Fig. 2(d) is consistent with the (011) pattern dominating as observed previously and the transmission electron microscopy (TEM) fringe pattern is consistent with the (011) pattern dominating as observed previously.[33] The FFT pattern suggests a separation of 3.54 nm^{-1} which suggests a lattice constant of 3.99 Å. The XRD pattern in Fig. 2E is closely matching literature data[34,35] for tetragonal $BaTiO_3$ (*P4mm*). The surface area of the particles measured with BET surface area 5.82 m^2 g^{-1} (Fig. 2F).

2.3. Immobilising barium titanate by PIM-EA-TB

An amount of 0.01 g barium titanate, a white crystal powder was combined 1 : 1 with a 2 mL solution of PIM-EA-TB (0.01 g) in chloroform. After 15 minutes of sonication, the suspension was drop-cast onto a 1 × 1 cm^2 filter paper (Whatman no. 1). The rapid evaporation of chloroform resulted in a uniform layer of PIM-EA-TB with embedded $BaTiO_3$, thereby forming an immobilized and easily recoverable/re-usable catalyst. Fig. 3 shows SEM images of the porous composite.

2.4. Quantification of H_2O_2 production

Hydrogen peroxide production and detection involved the reaction of 1 mg $BaTiO_3$, that was either (i) bare or (ii) embedded in PIM-EA-TB@$BaTiO_3$, with a 90% deionized water and typically 10% isopropanol solution. After a 5 minute reaction time, the sample solution was filtered or the catalyst removed, and the hydrogen peroxide concentration was quantified by mass spectroscopy indirectly *via* reaction with *para*-nitroboronic acid to *para*-nitrophenol (see ESI†).[36] Mass spectrometry (LC-MS) analyses were performed on an Automated Agilent QTOF (Walkup) used with HPLC (4 chromatography columns) and variable wavelength detector based on an Agilent QTOF 6545 with a Jetstream ESI† spray source coupled to an Agilent 1260 Infinity II Quat pump HPLC with a 1260 autosampler, and a column oven compartment and variable wavelength detector.

2.5. Electron paramagnetic resonance (EPR)

Electron paramagnetic resonance (EPR) spectroscopy measurements were performed on a Bruker Elexsys E500 spectrometer equipped with a Bruker ER4122-SHQE X band resonator. EPR spectra were recorded at either room temperature or 98 K and

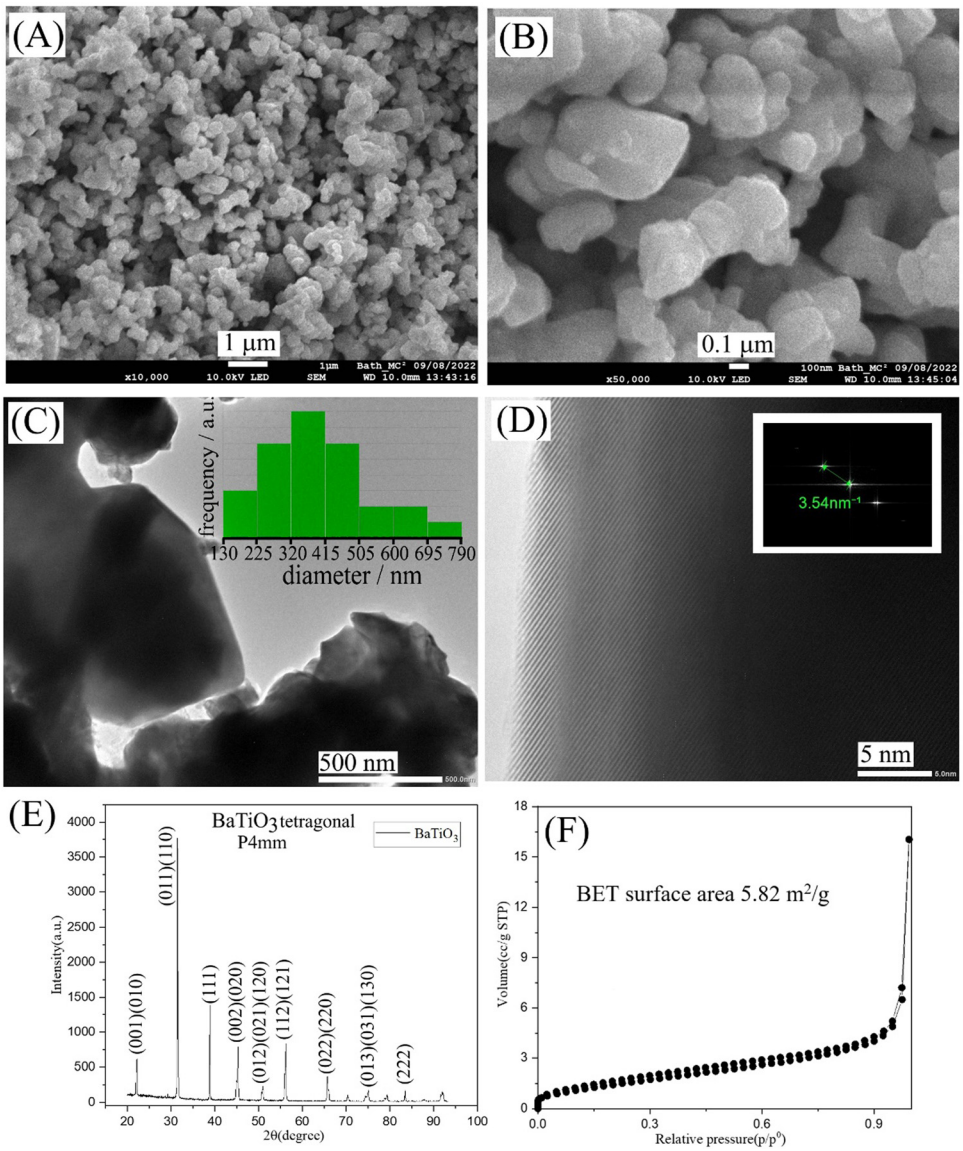

Fig. 2 (A) and (B) SEM images of $BaTiO_3$ particles with typically 0.37 ± 0.10 μm diameter. (C) and (D) TEM images showing $BaTiO_3$ aggregates and fringe pattern (Inset: Fourier transform with lattice constant 3.54 nm^{-1}.). (E) XRD pattern. (F) Nitrogen (BET) adsorption isotherm.

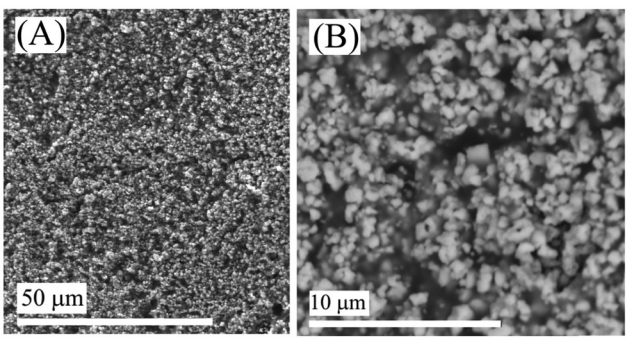

Fig. 3 (A) and (B) SEM images of $BaTiO_3$ particles (white) embedded into PIM-EA-TB (grey) in 1 : 1 weight ratio.

100 kHz magnetic field modulation frequency, 0.4 mT magnetic field modulation amplitude, 10.24 ms conversion time, 60 dB receiver gain, 4096 number of points, and 10 averages per spectrum. The powder samples were degassed overnight at 393 K under a dynamic vacuum in a Schlenk line prior to EPR measurements. EPR spectra were simulated using the Easyspin toolbox for Matlab.[37]

3. Results and discussion

3.1. Contrasting reactivity of bare and immobilised barium titanate

Initially, reactivity tests were performed with 1 mg $BaTiO_3$ catalyst suspended in 1 cm^3 water (containing 10 vol% isopropanol) with gentle agitation. Fig. 4A (red symbols) shows the production of H_2O_2 with time (thermocatalytic). An increase in

H_2O_2 concentration occurs over the first 30 minutes with a plateau probably due to simultaneous consumption of H_2O_2. Next, the same amount of catalyst powder immobilised within a PIM-EA-TB host polymer was deposited onto a cellulose substrate and placed into 1 cm^3 water (containing 10 vol% isopropanol) with only natural convection. Fig. 4A (black symbols) shows that the production of H_2O_2 under these conditions essentially doubles, despite using the same conditions and the same amount of catalyst. The process continues up to about 60 minutes, then reaching a plateau close to 0.3 mM H_2O_2. The plateau is likely to be associated with the competing reduction of H_2O_2 to water. Next, by purging the solution with pure oxygen (replacing ambient oxygen) the same reaction (Fig. 4A, blue symbols) leads to the formation of approx. 5 times more H_2O_2. That is, the process appears to be first order in oxygen. The mechanism can be written in two sequential reaction steps (eqn (1) and (2).

$$\text{Isopropanol} \rightleftarrows \text{acetone} + 2H^+(aq) + 2e^-(\text{barium titanate}) \quad (1)$$

$$O_2(aq) + 2H^+(aq) + 2e^-(\text{barium titanate}) \rightleftarrows H_2O_2(aq) \quad (2)$$

The mechanism is assigned to a surface process based on (i) isopropanol being oxidised and the transfer of two electrons into the conduction band (essentially interfacial Ti(III)), (ii) dioxygen from solution interacting with the $BaTiO_3$ surface and transfer of two electrons to form H_2O_2. This kind of process with a slow oxygen reduction reaction could be facilitated by the presence of protonated tertiary ammonium site on the PIM-EA-TB polymer backbone (see Fig. 1B) to explain the observed increase in catalytic rate. However, the pH within the polymeric structure is not well defined, and it might switch between two states during the course of the reaction cycle within the polymeric cages containing the barium titanate catalyst (*vide infra*). Next, the effect of the amount of catalyst was investigated. Fig. 4B shows good linearity with the amount of catalyst building up substantial concentrations of H_2O_2 for both the bare barium titanate catalyst and the PIM-EA-TB embedded catalyst. The rate of formation of H_2O_2 appears to be first order in $BaTiO_3$ surface sites. With the $BaTiO_3$ embedded into PIM-EA-TB, the rate of H_2O_2 production approximately doubles in all cases. The PIM-EA-TB polymer provides a microporous environment for effective diffusion of reagents. The molecular rigidity of the polymer prevents blocking of the catalyst surface sites.

The investigation of the effect of the amount of isopropanol is shown in Fig. 4C. When doubling the concentration of isopropanol from 10 vol% to 20 vol%, the rate of H_2O_2 production doubles. Therefore, the rate of H_2O_2 formation is first order in isopropanol for both the bare barium titanate catalyst

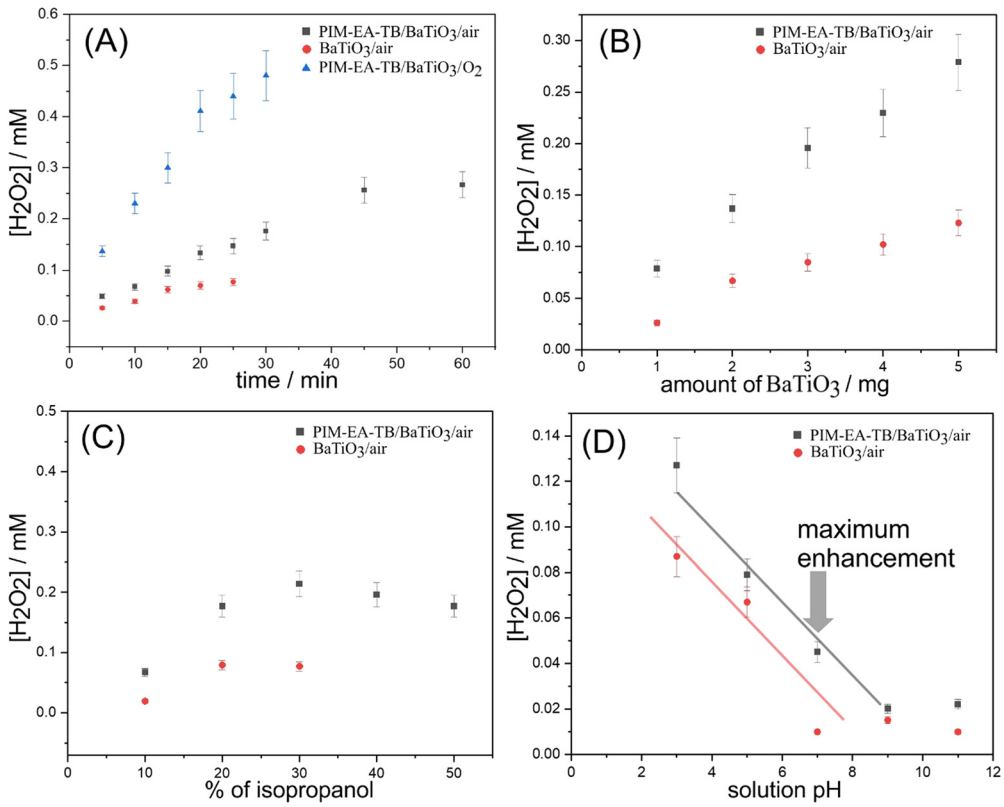

Fig. 4 (A) Production of H_2O_2 with time for 1 mg $BaTiO_3$ in 1 cm^3 water with 10 vol% isopropanol (square: with PIM-EA-TB; circle: pure catalyst; triangle: in pure oxygen). (B) Effect of the amount of catalyst in water with 10 vol% isopropanol; 5 min. (C) Effect of vol% isopropanol on H_2O_2 production for 1 mg $BaTiO_3$; 5 min. (D) Production of H_2O_2 with 1 mg $BaTiO_3$ in 1 cm^3 water with 10 vol% isopropanol as a function pH (adjusted by adding very small quantities of aqueous NaOH or HCl). Errors estimated at ±10%.

and PIM-EA-TB embedded catalyst. Only with very high concentrations of isopropanol of 30 vol% or higher is a plateau, or a decline, in H_2O_2 production observed. This is consistent with a process that is first order in isopropanol and saturation of surface sites. The presence of isopropanol at the catalyst surface could also slow down the oxygen reduction to result in this behaviour.

The effect of the solution pH (for 10 vol% isopropanol) is shown in Fig. 4D. Perhaps interestingly, the reaction does not work at all in the alkaline pH range (with or without polymer host). Only at a pH 6, or more acidic, is $BaTiO_3$ effective for oxygen reduction and H_2O_2 production. This observation matches with the reported point zero charge (pzc) at approx. pH 4.[38] Protonation of the surface could provide "docking sites" for oxygen reduction, but it might also affect the electron transfer from Ti(III) in the negatively charged interior to the positively charged surface. Furthermore, the protonation could affect the concentration of conduction band electrons (or Ti(III)) for electron transfer at the interface. In the presence of PIM-EA-TB, the effect is further enhanced, which is likely to be linked to the pK_A of the Tröger-base amine sites in the polymer backbone at approx. pH 4.[17] Protonation of the polymer backbone further enhances the rate of H_2O_2 production either (i) by providing protons during oxygen reduction or (ii) due to additional positive charges at the catalyst surface further enhancing electric field gradients (*i.e.* the rate of electron transfer). The most pronounced rate enhancement effects are observed close to pH 7 or in unbuffered media. The re-cycling of the barium titanate catalyst in PIM-EA-TB is demonstrated in Fig. S1 (ESI†).

3.2. Electron paramagnetic resonance (EPR) data for reactivity of immobilised barium titanate

EPR investigations of barium titanate provides a powerful tool to study chemical species.[39] Radical centres are observed for both bulk state and surface states and as a function of treatment. First, in order to establish the bulk properties, the barium titanate powder sample was heated and dried under vacuum and then investigated at 98 K (under vacuum to remove all surface species) with/without a 300 W mercury tungsten blended UV reflector (simulating the solar spectrum) to identify bulk EPR signals (Fig. 5). The EPR response is consistent with high temperature annealed barium titanate.[40]

The barium titanate powder measured at 98 K revealed the presence of Mn^{2+} trace impurities commonly found in barium titanate samples.[41] For the main signal, simulation revealed the presence of a signal exhibiting a *g*-tensor with axial symmetry and principal values equal to $g_\perp$ = 2.004 and $g_\parallel$ = 1.987. Kolodiazhnyi and Petric[41] attributed a similar signal to the presence of paramagnetic lattice vacancies. A reduction of the solid can be employed to build a higher concentration of these vacancies with a temperature dependent EPR signature.[42] Interestingly, the best linewidth fit of the simulated spectrum to the experimental spectrum could only be obtained when simulating two types of Ti vacancies with the same *g*-tensor principal values but different g strain line broadening. This could be the reflection of Ti vacancies in two slightly different crystallographic environments. Upon 35 minutes of irradiation of the powder barium titanate with a lamp having the same emission spectrum as the solar radiation, a further signal appeared at g = 1.942 (see * symbol). Kolodiazhnyi and Petric[41] and the literature cited therein attributed this g value to a further Ti^{3+} paramagnetic centres. Next, the same barium titanate nanopowder (without heating and vacuum) was investigated (Fig. 5C). All the spectra of the impregnated paper exhibit signals corresponding to the Ti vacancies and Ti^{3+} point defects as seen previously in the simulations. A shoulder or broadening denoted "**" towards lower magnetic induction (not in the range for Ti^{3+}) could be linked to surface states (associated with the oxygen species) or it could be associated with a Ti vacancy with broader line width. Both isopropanol treatment and

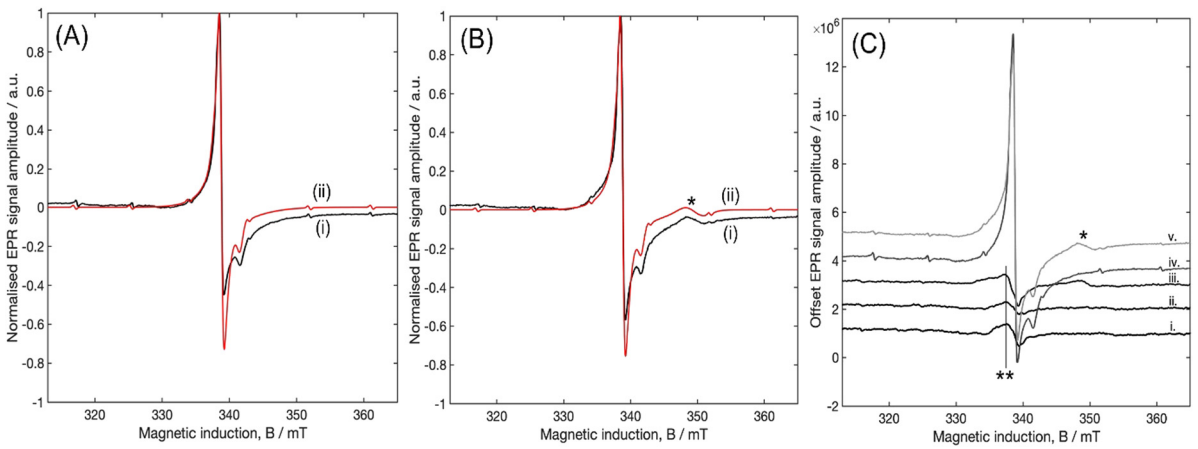

Fig. 5 (A) EPR experimental spectrum (i, black trace) and simulation (ii, red trace) of $BaTiO_3$ nanopowder (heated and retained under vacuum) at 98 K. (B) EPR experimental spectrum (i, black trace) and simulation (ii, red trace) of $BaTiO_3$ after 35 minutes of 300 W mercury tungsten blended UV reflector irradiation at 98 K. (C) EPR spectra of (i) $BaTiO_3$ PIM-EA-TB-embedded impregnated onto paper without solution; (ii) as before, wetted with a 30%v isopropanol aqueous solution; (iii) as before, wetted with a 30%v isopropanol aqueous solution after 35 minutes of 300 W mercury tungsten blended UV reflector irradiation; (iv) $BaTiO_3$ nanopowder; (v) $BaTiO_3$ powder after 35 minutes of irradiation. All the spectra were recorded at 98 K; (iv and v were heat treated under vacuum).

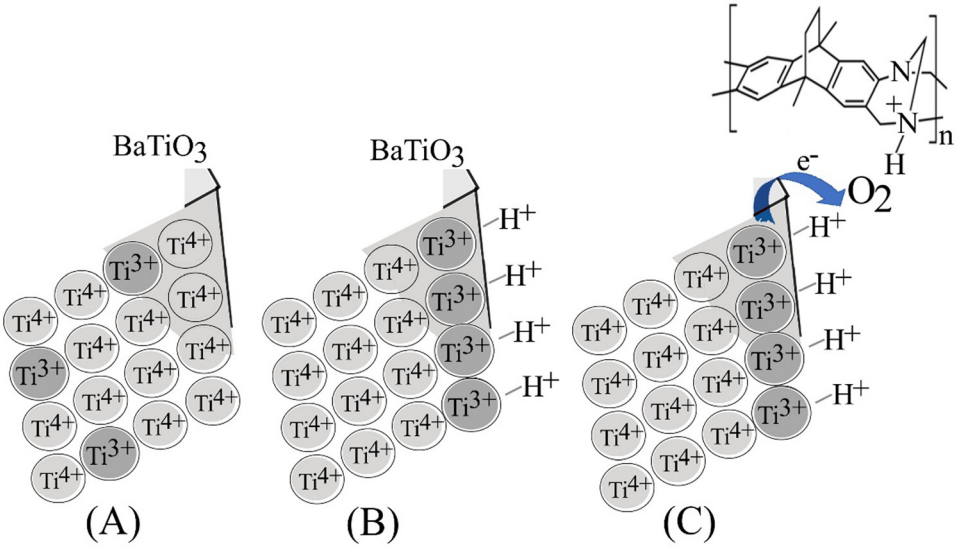

Fig. 6 Illustration of (A) the $BaTiO_3$ lattice, (B) the effect of protonation on double layer formation, and (C) the transition state for the oxygen reduction reaction.

exposure to light did not cause increase in the main signal (associated with the bulk).

3.3. Mechanistic model for reactivity of immobilised barium titanate

It seems likely that Ti(III) sites form at barium titanate interfaces, in particular in the presence of the reducing reagent isopropanol (eqn (1). The EPR signals did not reveal additional Ti(III) in the presence of isopropanol, but they might be dominated by bulk Ti(III) and are therefore less sensitive to surface states. The reduction of oxygen (eqn (2) then requires protons; probably involving protonation of both the barium titanate surface and the PIM-EA-TB host (see Fig. 4d). The reduction of oxygen requires two electrons (both from barium titanate) and two protons (enhanced by PIM-EA-TB protonation; Fig. 6). A similar pH-dependent change in reactivity related to the polymer cage was recently proposed for nano-Pd catalysts embedded in PIM-EA-TB.[23] The presence of the additional proton in the vicinity is proposed to accelerate electron tunnelling into O_2. The overall reaction (eqn (1) and (2) is pH neutral as the isopropanol oxidation can replenish both protons and electrons.

4. Conclusion

It has been shown that molecularly rigid polyamines (PIM-EA-TB) are able to host barium titanate nanoparticles for hydrogen peroxide production without capping or blocking of the catalytically active surface. Instead, an enhancement of the catalytic reaction occurs which is assigned here to a "cavity effect" inside the PIM-EA-TB that is essentially modulating the local cavity pH to switch between two states: (state 1) with the amine protonated (cavity pH < 4) the reduction of O_2 is favoured and (state 2) with the amine deprotonated (cavity pH > 4) the oxidation of iso-propanol is enhanced. Here, the reduction of O_2 is likely to be the rate limiting step and therefore the origin of the kinetic "cage" effect. There could be further kinetic effects of the PIM-EA-TB also on the catalytic decomposition of hydrogen peroxide (accompanying the formation of hydrogen peroxide), which will require further study in the future.

In the future, cavity effects in molecularly rigid host environments could be beneficial in a wider range of catalytic processes. A comparison of different polymers of intrinsic microporosity (and of other related host materials) could be useful to further explore/optimise molecular structure effects on cavity processes in catalysis. A more detailed study of similar catalytic and electrocatalytic systems will be required.

Data availability

The data supporting this article have been included as part of the ESI.†

Conflicts of interest

There are no conflicts to declare.

Acknowledgements

A. K. thanks the National Overseas Scholarship-India. F. M. thanks for the initial financial support by the EPSRC (EP/K004956/1). C. R. B. acknowledges support of UKRI Frontier Research Guarantee on "Processing of Smart Porous Electro-Ceramic Transducers – ProSPECT", project no. EP/X023265/1.

References

1 E. Lines and A. M. Glass, *Principles and applications of ferroelectrics and related materials*. Oxford University Press, Oxford, 1977.

2 T. Sakthivel, G. Venugopal, A. Durairaj, S. Vasanthkumar and X. Y. Huang, Utilization of the internal electric field in semiconductor photocatalysis: A short review, *J. Ind. Eng. Chem.*, 2019, **72**, 18–30.
3 S. K. Ray, J. Cho and J. Hur, A critical review on strategies for improving efficiency of BaTiO3-based photocatalysts for wastewater treatment, *J. Environ. Manage.*, 2021, **290**, 112679.
4 Q. Z. Zhang, Y. M. Jia, W. W. Wu, C. J. Pei, G. Q. Zhu, Z. S. Wu, L. H. Zhang, W. Fan and Z. Wu, Review on strategies toward efficient piezocatalysis of BaTiO3 nanomaterials for wastewater treatment through harvesting vibration energy, *Nano Energy*, 2023, **113**, 108507.
5 G. Panthi and M. Park, Approaches for enhancing the photocatalytic activities of barium titanate: A review, *J. Energy Chem.*, 2022, **73**, 160–188.
6 D. Sengupta, S. Naskar and D. Mandal, Reactive oxygen species for therapeutic application: Role of piezoelectric materials, *Phys. Chem. Chem. Phys.*, 2023, **25**(38), 25925–25941.
7 Q. Q. Xu, X. Y. Gao, S. F. Zhao, Y. N. Liu, D. Zhang, K. C. Zhou, H. Khanbareh, W. S. Chen, Y. Zhang and C. Bowen, Construction of bio-piezoelectric platforms: from structures and synthesis to applications, *Adv. Mater.*, 2021, **33**(27), 2008452.
8 Z. Y. Zhou, C. Zhan and E. J. Kan, Understanding the piezocatalytic properties of the BaTiO3 (001) surface via density functional theory, *Phys. Chem. Chem. Phys.*, 2023, **25**, 8631–8640.
9 M. A. Bin Adnan, K. Arifin, L. J. Minggu and M. B. Kassim, Titanate-based perovskites for photochemical and photoelectrochemical water splitting applications: a review, *Int. J. Hydrogen Energy*, 2018, **43**(52), 23209–23220.
10 M. Q. Wu, Z. Y. Zhang, Z. R. Liu, J. M. Zhang, Y. L. Zhang, Y. M. Ding, T. Huang, D. L. Xiang, Z. Wang, Y. J. Dai, X. Y. Wan, S. B. Wang, H. L. Qian, Q. J. Sun and L. L. Li, Piezoelectric nanocomposites for sonodynamic bacterial elimination and wound healing, *Nano Today*, 2021, **37**, 101104.
11 G. Prasanna, H. D. P. Nguyen, S. Dunn, A. Karunakaran, F. Marken, C. R. Bowen, B. N. T. Le, H. D. Nguyen and T. P. T. Pham, Impact of stirring regime on piezocatalytic dye degradation using BaTiO3 nanoparticles, *Nano Energy*, 2023, **116**, 108794.
12 R. A. Surmenev, T. Orlova, R. V. Chernozem, A. A. Ivanova, A. Bartasyte, S. Mathur and M. A. Surmeneva, Hybrid lead-free polymer-based nanocomposites with improved piezoelectric response for biomedical energy-harvesting applications: A review, *Nano Energy*, 2019, **62**, 475–506.
13 Z. X. Low, P. M. Budd, N. B. McKeown and D. A. Patterson, Gas permeation properties, physical aging, and its mitigation in high free volume glassy polymers, *Chem. Rev.*, 2018, **118**(12), 5871–5911.
14 N. B. McKeown and P. M. Budd, Polymers of intrinsic microporosity (PIMs): organic materials for membrane separations, heterogeneous catalysis and hydrogen storage, *Chem. Soc. Rev.*, 2006, **35**, 675–683.
15 Z. K. Li, R. Malpass-Evans, N. B. McKeown, M. Carta, K. Mathwig, J. P. Lowe and F. Marken, Effective electroosmotic transport of water in an intrinsically microporous polyamine (PIM-EA-TB), *Electrochem. Commun.*, 2021, **130**, 107110.
16 F. J. Xia, M. Pan, S. C. Mu, R. Malpass-Evans, M. Carta, N. B. McKeown, G. A. Attard, A. Brew, D. J. Morgan and F. Marken, Polymers of intrinsic microporosity in electrocatalysis: novel pore rigidity effects and lamella palladium growth, *Electrochim. Acta*, 2014, **128**, 3–9.
17 E. Madrid, Y. Y. Rong, M. Carta, N. B. McKeown, R. Malpass-Evans, G. A. Attard, T. J. Clarke, S. H. Taylor, Y.-T. Long and F. Marken, Metastable ionic diodes derived from an amine-based polymer of intrinsic microporosity, *Angew. Chem., Int. Ed.*, 2014, **53**(40), 10751–10754.
18 D. P. He, D. S. He, J. L. Yang, Z. X. Low, R. Malpass-Evans, M. Carta, N. N. McKeown and F. Marken, Molecularly rigid microporous polyamine captures and stabilizes conducting platinum nanoparticle networks, *ACS Appl. Mater. Interfaces*, 2016, **8**(34), 22425–22430.
19 F. Marken, L. N. Wang, Y. Z. Zhao, Z. K. Li, M. Amiri and H. Imanzadeh, Polymers of intrinsic microporosity (PIMs) in sensing and in electroanalysis, *Curr. Opin. Chem. Eng.*, 2022, **35**, 100765.
20 Y. Z. Zhao, J. Dobson, C. Harabajiu, E. Madrid, T. Kanyanee, C. Lyall, S. Reeksting, M. Carta, N. B. McKeown, L. Torrente-Murciano, K. Black and F. Marken, Indirect photoelectrochemical detection of carbohydrates with Pt@g-C_3N_4 immobilised into a polymer of intrinsic microporosity (PIM-1) and attached to a palladium hydrogen capture membrane, *Bioelectrochemistry*, 2020, **134**, 107499.
21 A. Karunakaran, K. J. Francis, C. R. Bowen, R. J. Ball, Y. Z. Zhao, L. N. Wang, N. B. McKeown, M. Carta, P. J. Fletcher, R. Castaing, M. A. Isaacs, L. J. Hardwick, G. Cabello, I. V. Sazanovich and F. Marken, Nanophase-photocatalysis: loading, storing, and release of H_2O_2 using graphitic carbon nitride, *Chem. Commun.*, 2023, **59**(48), 7423–7426.
22 S. D. Ahn, A. Kolodziej, R. Malpass-Evans, M. Carta, N. B. McKeown, S. D. Bull, A. Buchard and F. Marken, Polymer of intrinsic microporosity induces host-guest substrate selectivity in heterogeneous 4-benzoyloxy-TEMPO-catalysed alcohol oxidations, *Electrocatalysis*, 2016, **7**(1), 70–78.
23 L. N. Wang, M. Carta, R. Malpass-Evans, N. B. McKeown, P. J. Fletcher, P. Estrela, A. Roldan and F. Marken, Artificial formate oxidase reactivity with nano-palladium embedded in intrinsically microporous polyamine (Pd@PIM-EA-TB) driving the H_2O_2-3,5,3',5'-tetramethylbenzidine (TMB) colour reaction, *J. Catal.*, 2022, **416**, 253–266.
24 M. Schrader, D. Mienert, T.-S. Oh, H.-I. Yoo and K. D. Becker, An optical, EPR and electrical conductivity study of blue barium titanate, BaTiO3−δ, *Solid State Sci.*, 2008, **10**(6), 768–775.
25 G. H. Kwei, A. C. Lawson, S. J. L. Billinge and S. W. Cheong, Structures of the ferroelectric phases of barium titanate, *J. Phys. Chem.*, 1993, **97**(10), 2368–2377.
26 H. C. Gao, Y. G. Zhang, H. Y. Xia, X. J. Zhu, X. X. Mao, W. R. Zhao, S. H. Miao and M. Q. Shi, In situ generation of H_2O_2 over Ce-doped BaTiO3 catalysts for enhanced piezo-photocatalytic degradation of pollutants in aqueous solution, *Colloids Surf., A*, 2023, **663**, 131030.

27 H. C. Gao, Y. Han, Y. Wang, H. Y. Xia, X. J. Zhu, D. J. Wang, Y. G. Zhang, X. X. Mao and L. J. Zhang, Dissolved oxygen enhanced piezo-photocatalytic performance in Ag dots-modified BaTiO3 nanoparticles for efficient degradation of multiple organic pollutants, *Sep. Purif. Technol.*, 2024, **346**, 127548.
28 W. Q. Qian, K. Zhao, D. Zhang, C. R. Bowen, Y. H. Wang and Y. Yang, Piezoelectric material-polymer composite porous foam for efficient dye degradation via the piezo-catalytic effect, *ACS Appl. Mater. Interfaces*, 2019, **11**(31), 27862–27869.
29 S. W. Xu, W. Q. Qian, D. Zhang, X. Zhao, X. M. Zhang, C. B. Li, C. R. Bowen and Y. Yang, A coupled photo-piezo-catalytic effect in a BST-PDMS porous foam for enhanced dye wastewater degradation, *Nano Energy*, 2020, **77**, 105305.
30 L. C. Wan, W. R. Tian, N. J. Li, D. Y. Chen, Q. F. Xu, H. Li, J. H. He and J. M. Lu, Hydrophilic porous PVDF membrane embedded with BaTiO3 featuring controlled oxygen vacancies for piezocatalytic water cleaning, *Nano Energy*, 2022, **94**, 106930.
31 M. Carta, R. Malpass-Evans, M. Croad, Y. Rogan, J. C. Jansen, P. Bernardo, F. Bazzarelli and N. B. McKeown, An efficient polymer molecular sieve for membrane gas separations, *Science*, 2023, **339**, 303–307.
32 G. Prasanna, H. D. P. Nguyen, S. Dunn, A. Karunakaran, F. Marken, C. R. Bowen, B. N. T. Le, H. D. Nguyen and T. P. T. Pham, Impact of stirring regime on piezocatalytic dye degradation using BaTiO3 nanoparticles, *Nano Energy*, 2023, **116**, 108794.
33 Y. Zhou, C. S. Park, C. H. Wu, D. Maurya, M. Murayama, A. Kumar, R. S. Katiyar and S. Priya, Microstructure and surface morphology evolution of pulsed laser deposited piezoelectric BaTiO3 films, *J. Mater. Chem. C*, 2013, **1**(39), 6308–6315.
34 D. Mewada, and Barium titanate (BaTiO3): A study of structural, optical and dielectric properties, *Mater. Today: Proc.*, 2022, **54**(3), 923–926.
35 S. Merrad, M. Abbas, R. Brahimi, B. Bellal and M. Trari, Synthesis, characterization and application of tetragonal BaTiO3-δ in adsorption and photocatalysis of Congo Red, *Mater. Today Commun.*, 2023, **35**, 105958.
36 L. N. Wang, M. Carta, R. Malpass-Evans, N. B. McKeown, P. J. Fletcher, D. Lednitzky and F. Marken, Hydrogen peroxide versus hydrogen generation at bipolar Pd/Au nanocatalysts grown into an intrinsically microporous polyamine (PIM-EA-TB), *Electrocatalysis*, 2021, **12**(6), 771–784.
37 S. Stoll and A. Schweiger, EasySpin, a comprehensive software package for spectral simulation and analysis in EPR, *J. Magn. Reson.*, 2006, **178**(1), 42–55.
38 M. Zeng, Surface reaction characteristics at low temperature synthesis BaTiO3 particles by barium hydroxide aqueous solution and titanium tetraisopropoxide, *Appl. Surf. Sci.*, 2011, **257**(15), 6636–6643.
39 R. N. Schwartz, B. A. Wechsler and D. Rytz, Electron-paramagnetic resonance, optical, and electronic-structure studies of photorefractive barium-titanate, *J. Amer. Ceramic Soc*, 1990, **73**(11), 3200–3205.
40 E. Neige and O. Diwald, Paramagnetic electron centers in BaTiO3 nanoparticle powders, *Phys. Chem. Chem. Phys.*, 2021, **23**(22), 12881–12888.
41 T. Kolodiazhnyi and A. Petric, Analysis of point defects in polycrystalline BaTiO3 by electron paramagnetic resonance, *J. Phys. Chem. Solids*, 2003, **64**(6), 953–960.
42 M. Schrader, D. Mienert, T. S. Oh, H. I. Yoo and K. D. Becker, An optical, EPR and electrical conductivity study of blue barium titanate, BaTiO3-δ, *Solid State Sci.*, 2008, **10**(6), 768–775.

